

Gravity Drainage of Bitumen Induced by Solvent Leaching

Mohammadjavad Mohammadi, Nasser Sabet, and Hassan Hassanzadeh*

Cite This: <https://doi.org/10.1021/acsomega.2c07634>

Read Online

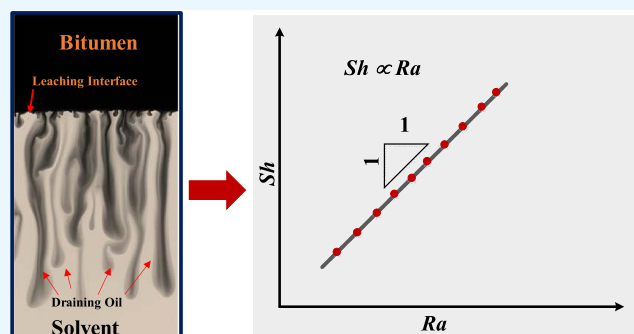
ACCESS |

Metrics & More

Article Recommendations

ABSTRACT: Steam-based thermal recovery processes are energy-intensive and pose environmental concerns due to their high greenhouse gas emissions. The application of solvents has shown promise in reducing the environmental impact of these processes. In this work, the solvent chamber theory is used to study the gravity drainage of bitumen. The results reveal that the drainage rate can be scaled using the thermophysical properties of solvents. The drainage rate is shown to be directly related to the density difference between bitumen and solvent and inversely proportional to the mixture viscosity. A universal scaling relation between the Sherwood number, as a measure of the mass transfer, and Rayleigh number, as a measure of the natural convection, in the form of $Sh = \beta Ra$ is presented using the experimental data of various solvents.

This linear relationship is consistent with the theoretical studies of buoyancy-driven convection. Moreover, the scaling prefactor β is found to decrease with increasing natural log of the mobility ratio (α), which results in a lower rate of convective mass transfer. Furthermore, a new critical Rayleigh number equation based on the power-law mixing rule (PLMR) is derived, and the results are compared with the available theories in the literature based on the exponential mixing rule (EMR). The findings provide insights into understanding the convective dissolution with large viscosity contrast. Furthermore, the developed scaling relation provides a useful tool to predict the convective mixing of different bitumen/solvent systems. The results find application in the design of the solvent-based bitumen recovery processes.



1. INTRODUCTION

Among various types of recovery methods for bitumen, steam-based processes are the most widely used due to their proven success in field-scale operations.^{1,2} In this regard, in situ thermal recovery processes, including steam flooding (SF), cyclic steam stimulation (CSS), and steam-assisted gravity drainage (SAGD), have been implemented on the field scale to recover bitumen from oil sands. However, the selection of the proper techniques depends on various factors such as geology, oil viscosity, and the initial reservoir conditions.³ Despite the popularity of these methods for bitumen extraction, their high energy intensity and greenhouse gas (GHG) emissions have remained a challenge.^{4,5} To address these issues, the so-called hybrid processes⁶ were introduced where a solvent is co-injected along with steam into the reservoirs to enhance the oil recovery by taking advantage of both heat and mass transfer mechanisms simultaneously. This, in turn, reduces steam–oil ratio, energy intensity, and GHG emissions. Furthermore, the pure solvent injection is used in the VAPor-EXtraction (also known as VAPEX) process⁷ to take advantage of mass transfer and gravity drainage, and also suggested as an efficient method for the oil recovery enhancement from naturally fractured heavy oil and bitumen reservoirs.^{8–10} Experimental studies of VAPEX in a two-dimensional (2D) sandpack using propane/

bitumen and butane/bitumen systems by Das and Butler¹¹ concluded that the production rate for counter-current contact configuration is about 2–3 times faster than the lateral contact configuration. Additionally, it was inferred that the presence of deasphalting during the process not only increases the production rate but also results in the upgrading of the produced oil.

There have been many numerical and experimental studies on solvent co-injection with steam since the solvent-aided process was introduced. Both liquid and gaseous solvents have been suggested^{6,12,13} and implemented in the pilot- or field-scale applications.^{14,15} The solvents that have been used or suggested for expanding-solvent-SAGD (ES-SAGD) include but are not limited to methane,¹⁶ ethane,^{16,17} propane,^{16–18} ethyl acetate (EA),^{19,20} dimethyl ether (DME),^{12,21–24} carbon dioxide (CO₂),¹⁷ naphtha,¹⁷ butane,^{16,25} pentane,²⁵ hexane,^{6,25–27} heptane,²⁵ and diluent (mixtures of C₄–C₁₀).²⁸

Received: November 29, 2022

Accepted: January 5, 2023

For example, Zirahi et al.^{19,20} used EA as a bio-based solvent to perform 2D physical model experiments and simulation studies. They concluded that 2–8 mol % of EA and steam can increase the production rate by 3–25% and reduce the steam–oil ratio (SOR) by 0.9 units. Furthermore, their 2D physical model experiments have indicated that the SOR can be reduced significantly compared to the SAGD. In addition, various efforts have been made to develop selection criteria for the co-injection of solvents with steam.^{13,29–31} For instance, Sabet et al.²⁹ studied the effect of different solvents on the onset of convective dissolution, and the results showed that solvents with a carbon number in the range of 7–9 provide an earlier onset of convective dissolution, which in turn improve the bitumen recovery.

Many experimental and simulation studies on the solvent-aided processes have focused on the type of solvent, the amount of solvent used, and their effects on the production rate.^{12,19,20,22,23,25,26,29} In contrast, bitumen leaching by solvents has rarely been studied. The numerical simulation studies reported in the literature have mainly employed large grid blocks where fundamental mechanisms such as viscosity- and density-driven fingering cannot be properly captured.³² When a heavier fluid is placed on top of a lighter one, the system is prone to buoyancy-driven instability named Rayleigh–Taylor (RT) instability.^{33–35} In this situation, the mixed heavier fluid at the top sinks down and the lighter fluid at the bottom floats up, enhancing the mixing process. When a bitumen column is contacted by solvent from beneath, RT convection plays a significant role in leaching bitumen from the interface, allowing solvents to penetrate deep into the virgin bitumen. For the first time, Mokrys³⁸ and Mokrys and Butler^{36,37} observed the natural convection in bitumen leaching when they conducted experiments using the Hele-Shaw cell for the bitumen/toluene system. They noted that the bitumen drainage rate is constant throughout the process, and moreover, it varies linearly with the permeability of the Hele-Shaw cell. In a highly fine-grid simulation reported by Salas et al.,³² the same bitumen drainage behavior was observed for a propane/bitumen system at 50 and 100 °C. Recently, Sabet et al.³⁹ studied the Rayleigh–Taylor instability at large viscosity ratios and concluded that beyond a critical viscosity ratio, the symmetry of the buoyancy-driven fingers breaks down and the downward fingers predominate. Nenniger and Dunn⁴⁰ used a data set of 60 individual rate measurements, including 11 crude oils, four solvents, a permeability range of 1.5–5400 Darcy, and a viscosity range of 90–800,000 mPa·s, to develop a correlation for the prediction of bitumen production rates for solvent-based gravity drainage. However, the impact of solvent density has not been captured, and hence the developed correlation does not provide a universal scaling relation. Therefore, a general scaling relation based on controlled experiments is lacking.

The main objective of this work is to study the performance of various solvents for bitumen leaching using the solvent chamber theory developed by Mokrys³⁸ and Mokrys and Butler.³⁷ Moreover, we intend to present a universal scaling relation that can be used for the design of experiments and numerical simulation studies of the gravity drainage processes involved in bitumen leaching by solvents.

This paper is organized as follows: In Section 2, the physics of the problem will be defined, and the employed mathematical model will be presented. Next, in Section 3, the main results obtained from the proposed model for various bitumen/

solvent systems will be discussed and compared. Finally, a brief summary and the main conclusions of the work are presented.

2. DESCRIPTION OF THE PROBLEM

Placement of a light fluid like a solvent beneath a column of bitumen in a Hele-Shaw cell leads to upward diffusion of the solvent into the bitumen column and growth of a mass transfer boundary layer. The developed boundary layer forms a gravitationally unstable mixing zone with several orders of magnitude viscosity variation leading to RT instabilities due to the density and viscosity differences. In this regard, the concentration dependencies of viscosity and density lead to complex density-driven fingering.³⁹ Figure 1 shows a schematic of the described configuration.

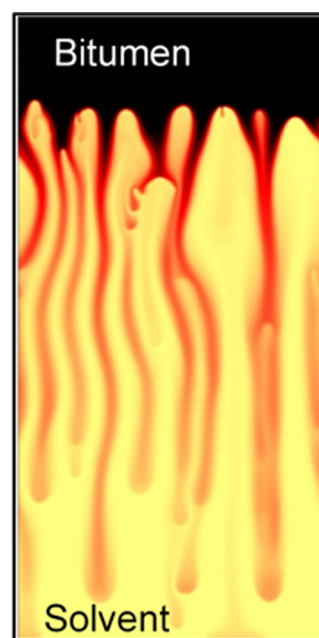


Figure 1. Schematic of fingering when a light fluid is placed underneath a heavy one. The two fluids are miscible. Reprinted in part with permission from ref 39. Copyright 2021 American Physical Society.

Mokrys and Butler^{36–38} studied bitumen leaching in a Hele-Shaw cell where bitumen (a highly viscous and dense fluid) and toluene (a less viscous and less dense fluid) are brought in contact. They also developed theoretical models to describe the experimental observations. Their models include simple counter-current flow, concentration gradient, and solvent chamber theory. The details of each model are summarized in Table 1. The focus of this work is on the solvent chamber theory model.

In the solvent chamber theory, the whole interface between solvent and bitumen rises with a steady-state velocity. The mass transfer occurs across a boundary layer that is surrounded by the lower and upper fronts or the so-called shock fronts by Mokrys³⁸ and Mokrys and Butler.^{36,37} The lower shock front is a boundary where the solvent concentration is maximum and corresponds to the minimum potential gradient. In contrast, the upper shock front is a boundary where the potential gradient is maximum with a minimum solvent concentration. It was assumed that the convective transfer above the upper shock front is negligible since the virgin bitumen is practically

Table 1. Developed Models of the Bitumen Leaching Process in a Hele-Shaw Cell by Mokrys and Butler^{36–38} along with the Considered Assumptions^{a,b,c}

model	submodel	assumptions
simple counter-current flow		only convection is involved no diffusion and no boundary layer exist
concentration gradient models	linear	a linear solvent concentration profile across the boundary layer is assumed: $c_s(\xi) = 1 - \xi/\xi_{\max}$ a boundary layer exists, but the diffusion effect is excluded solvent concentration range: $c_s = 0.05-1$
	exponential	an exponential solvent concentration profile across the boundary layer: $c_s(\xi) = \exp(-2.996\xi/\xi_{\max})$ a boundary layer exists, but the diffusion effect is excluded solvent concentration range: $c_s = 0.05-1$
	linear step function	a linear step function solvent concentration profile across the boundary layer is assumed: $c_s(\xi) = c_{\max} - \frac{c_{\max} - c_{\min}}{\xi_{\max}} \xi$ a boundary layer exists, but the diffusion effect is excluded solvent concentration range: $c_{\min} < c_s < c_{\max}$ where c_{\min} and c_{\max} are assumed
solvent chamber theory		diffusion controls the drainage flow across the boundary layer a parabolic shape of the finger is assumed solvent concentration range: $c_{\min} < c_s < c_{\max}$ where c_{\min} and c_{\max} are determined using mass balance

^a c_s : solvent volume fraction. ^b ξ : normal distance in the boundary layer. ^c ξ_{\max} : width of the boundary layer.

immobile. As solvent diffuses upward into the bitumen column, the diffusion flux of solvent is balanced by the downward flux (drainage) of the diluted bitumen.

The solvent chamber theory works based on the determination of the solvent concentration at lower and upper shock fronts and subsequently consideration of mass balance equations across the boundary layer. It is worthwhile mentioning that based on the experimental observations, Mokrys and Butler^{36–38} used a parabolic shape of a finger to develop the mass balance across the boundary layer. The details of the development of the model can be found elsewhere.³⁸ The interfacial velocity is obtained as

$$U = Kg(\rho_b - \rho_s) \frac{[I_3 - (1 - c_{\max})I_2]}{I_1} \quad (1)$$

where U is the interface velocity; K is the permeability of the Hele-Shaw cell; ρ_b and ρ_s are the density of bitumen and solvent, respectively; c_{\max} is the solvent concentration at the lower shock front; and I_1 , I_2 , and I_3 are the integral constants and depend on the bitumen/solvent system, as defined in the following

$$I_1 = \int_{c_{\min}}^{c_{\max}} \frac{D_s}{c_s} dc_s \quad (2)$$

$$I_2 = \int_{c_{\min}}^{c_{\max}} \frac{D_s(1 - c_s)}{\mu c_s} dc_s \quad (3)$$

$$I_3 = \int_{c_{\min}}^{c_{\max}} \frac{D_s(1 - c_s)^2}{\mu c_s} dc_s \quad (4)$$

In these equations, D_s is the diffusion coefficient of solvent in bitumen and can be either constant or dependent on concentration; c_{\min} is the solvent concentration at the upper shock front; and c_{\min} and c_{\max} can be determined by applying mass balance at the upper and lower shock fronts.

It should be noted that c_{\min} is a concentration where the function $f(c_s) = c_s\mu/(1 - c_s)$ is maximum and c_{\max} corresponds to a concentration at which the mixture viscosity (μ) is equal to $(1 + c_s)\mu_s$, where μ_s is the pure solvent viscosity. When the diffusion coefficient of the solvent is assumed to be constant, it will be canceled out from I_1 , I_2 , and I_3 in eq 1. Therefore, eq 1 reduces to

$$U = Kg\Delta\rho \frac{[I'_3 - (1 - c_{\max})I'_2]}{I'_1} \quad (5)$$

where $\Delta\rho = \rho_b - \rho_s$, $I'_1 = \int_{c_{\min}}^{c_{\max}} dc_s/c_s$, $I'_2 = \int_{c_{\min}}^{c_{\max}} [(1 - c_s)/\mu c_s] dc_s$, $I'_3 = \int_{c_{\min}}^{c_{\max}} [(1 - c_s)^2/\mu c_s] dc_s$.

According to the experimental works carried out by Mokrys et al.,³⁸ the boundary layer moves upward at a steady velocity (U). Therefore, this interface motion provides a direct measure of the convective mass flux, as given by⁴¹

$$F_c = \phi U \Delta c \quad (6)$$

where ϕ is the porosity, U is the interfacial velocity, and Δc is the concentration difference between pure solvent and bitumen/solvent mixture. A pure convective flux is independent of the draining diluted oil position and depends only on the Rayleigh number,^{41,42} $Ra = \nu H/\phi D_s$, where H is the depth of the Hele-Shaw cell, D is the molecular diffusivity, and $\nu = Kg\Delta\rho/\mu_s$ is the natural buoyancy flux. The dimensionless flux is defined as the Sherwood number $Sh = F_c H/\phi D_s \Delta c$ or in a simpler form $Sh = UH/D_s$.

Multiplying eq 1 by $H/D_s\mu_s$ and doing some algebra (see Appendix for more details), we arrive at

$$Sh = \beta Ra \quad (7)$$

where $Sh = UH/D_s$, $Ra = \nu H/D_s = Kg\Delta\rho H/\mu_s D_s$, and $\beta = [I'_{D3} - (1 - c_{\max})I'_{D2}]/I'_1$.

I'_1 is remained unchanged (as defined in eq 2) and I'_{D2} , I'_{D3} will be

$$I'_{D2} = \int_{c_{\min}}^{c_{\max}} \frac{(1 - c_s)}{\mu_D c_s} dc_s \quad (8)$$

$$I'_{D3} = \int_{c_{\min}}^{c_{\max}} \frac{(1 - c_s)^2}{\mu_D c_s} dc_s \quad (9)$$

where dimensionless viscosity is $\mu_D = \mu/\mu_s$. It should be noted that β is a dimensionless parameter and depends on the physical properties of both heavy and light fluids in the system.

3. RESULTS AND DISCUSSION

Bitumen at reservoir conditions is immobile and highly viscous with viscosities in the order of millions. When immobile bitumen comes into contact with a solvent that is either fully miscible or partially miscible, the solvent diffuses into the bitumen, dilutes it, and makes it mobile. The same behavior is observed in gravity drainage of bitumen resulting from leaching once the solvent contacts the viscous bitumen column from

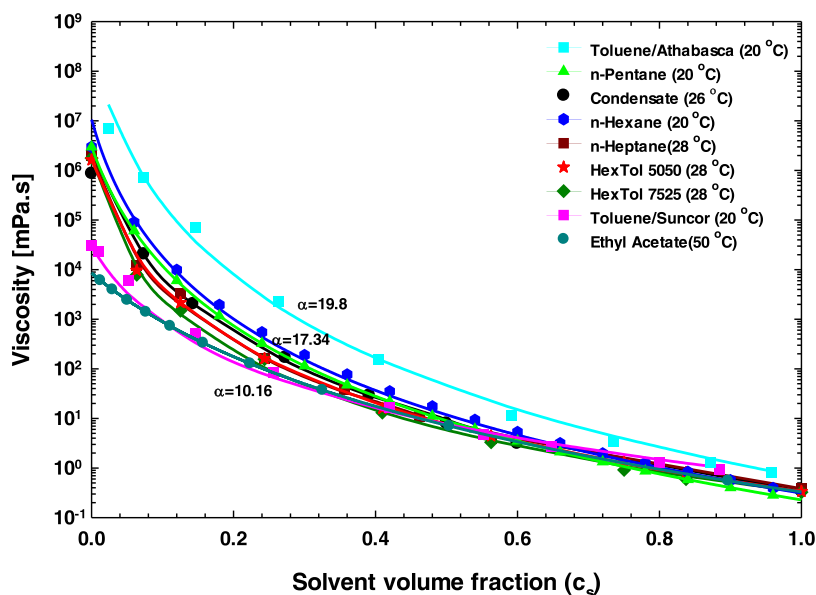


Figure 2. Viscosity of various bitumen/solvent mixtures vs the solvent volume fraction. Mixture viscosity data for Athabasca/toluene and Suncor/toluene are obtained from the studies of Mokrys et al.,³⁸ MacKay/n-pentane and MacKay/n-hexane from Haddadnia et al.,⁵³ Surmont/n-heptane and Surmont/condensate from Nourozieh et al.,⁵⁴ and Nourozieh et al.,⁵⁵ respectively; MacKay/ethyl acetate from Zirahi et al.,¹⁹ and MacKay/Hextol 5050 and MacKay/Hextol 7525 are measured data in this work. The symbols show the experimental data, and the lines represent the predicted viscosity values using power-law mixing rule for each set of solvent/bitumen system.

below. Initially, the solvent diffuses into bitumen, creates a diffusive unstable boundary layer, and further reduces bitumen viscosity and density leading to the drainage process.

The Rayleigh number, which is defined as the ratio of buoyancy forces over diffusive forces, is a key dimensionless group that characterizes buoyancy-driven flows.⁴³ The onset of natural convection can be predicted by linear stability analysis (LSA). The critical Rayleigh number (Ra_c) is a constant that signifies a limit below which the system remains stable (diffusive mass transfer prevails).^{32,44} On the other hand, a system with a Ra greater than Ra_c could lead to convective instabilities.

For a constant-viscosity system, the critical Ra number is $4\pi^2$,^{45,46} while for a system with concentration-dependent viscosity, the critical Ra defined based on more viscous fluid (here, bitumen with μ_b) is considerably below $4\pi^2$.^{47,48} This phenomenon was observed experimentally by Butler et al.,⁴⁹ but they did not provide a theoretical explanation about why convection currents are observed at a Ra below the critical value of $4\pi^2$. Sabet et al.^{47,50} and Rabiei et al.⁴⁸ derived an equation for the critical Rayleigh number using linear stability analysis for different mixtures for the classical Horton–Rogers–Lapwood problem.^{45,46} It is worthwhile mentioning that they^{47,48,50} proposed the model based on the exponential viscosity mixing rule (EMR) as $\mu = \mu_b e^{-\alpha X_s}$ or $\mu = \mu_s e^{-\alpha(1-X_s)}$, where X_s is the solvent mole fraction. The proposed equation provides valuable insight into the significance of viscosity variation in the development of convective instabilities and the critical Rayleigh number, defined based on the viscosity of bitumen (μ_b), is given by

$$Ra_c = 4\pi^2 \left[1 + \frac{\alpha^2}{4\pi^2} \right] \frac{\alpha}{[e^\alpha - 1]} \quad (10)$$

If the Rayleigh number is defined according to the viscosity of less viscous fluid (here, solvent with μ_s), the critical Rayleigh number will be

$$Ra_c = 4\pi^2 \left[1 + \frac{\alpha^2}{4\pi^2} \right] \frac{\alpha}{[1 - e^{-\alpha}]} \quad (11)$$

where $M = \mu_b/\mu_s$ is the mobility ratio and $\alpha = \ln M$ is a constant that characterizes the behavior of mixture viscosity vs solvent concentration.

In this work, the power-law mixing rule (PLMR), $\mu = \mu_s [(1 - c_s)e^{\alpha n} + c_s]^{1/n}$, is used for viscosity calculations, where n is a fitting parameter and c_s is the solvent volume fraction since it provides a better fit with the experimental data.^{51,52} A new equation for critical Rayleigh number based on the power-law mixing rule (PLMR) is introduced using linear stability analysis (LSA). The marginal instability condition for the classical Horton–Rogers–Lapwood problem^{45,46} gives the critical Rayleigh number as

$$Ra_c = \frac{4\pi^2 + X_{II}}{F_{II}} \quad (12)$$

where F_{II} and X_{II} are

$$F_{II} = 2 \int_0^1 \frac{\sin^2(\pi z_D)}{\mu_D} dz_D \quad (13)$$

$$X_{II} = Y_{II} \int_0^1 \frac{\sin^2(\pi z_D)}{\mu_D^n} dz_D \quad (14)$$

and Y_{II} depends on the definition of critical Rayleigh number. Thus, based on the viscosity of bitumen (μ_b),

$$Y_{II} = 2\pi \left[\frac{1 - e^{-\alpha n}}{n} \right] \quad (15)$$

and based on the viscosity of solvent (μ_s),

$$Y_{II} = 2\pi \left[\frac{e^{\alpha n} - 1}{n} \right] \quad (16)$$

Table 2. Viscosity Power-Law Mixing Rule Fitting Parameters and the Natural Log of Mobility Ratios for Various Bitumen/Solvent Mixtures

bitumen	solvent	α	n	R^2	temperature [°C]	ref
Athabasca	toluene	19.8	-0.1532	1	20	Mokrys et al. ³⁸
MacKay	<i>n</i> -pentane	18.23	-0.1730	0.9865	20	Haddadnia et al. ⁵³
Surmont	condensate ^a	15.7	-0.1955	0.9994	26	Nourozieh et al. ⁵⁵
MacKay	<i>n</i> -hexane	17.34	-0.1786	0.9934	20	Haddadnia et al. ⁵³
Surmont	<i>n</i> -heptane	15.45	-0.2169	0.9872	28	Nourozieh et al. ⁵⁴
MacKay	hextol 5050 ^b	15.39	-0.2088	0.9981	28	this work
MacKay	hextol 7525 ^c	15.51	-0.2299	0.9912	28	this work
Suncor	toluene	10.72	-0.2591	1	20	Mokrys et al. ³⁸
MacKay	ethyl acetate	10.16	-0.1724	0.9921	50	Zirahi et al. ¹⁹

^aCondensate: *n*-C5 (35.73 wt %), *n*-C6 (25.29 wt %), *n*-C7 (21.92 wt %), and C8⁺ (17.06 wt %). ^bHextol 5050: *n*-C6 (50 wt %) and toluene (50 wt %). ^cHextol 7525: *n*-C6 (75 wt %) and toluene (25 wt %).

where $\mu_D(z_D) = \mu(z_D)/\mu_s$ or $\mu_D(z_D) = \mu(z_D)/\mu_b$ is the dimensionless viscosity of the mixture corresponding to the steady-state concentration profile given by $c_s = 1 - z_D$, and z_D represents the vertical coordinate direction.

The details of LSA formulation can be found elsewhere.^{47,50} Depending on the definition of dimensionless viscosity, based on the solvent viscosity ($\mu_D = \mu/\mu_s = [(1 - c_s)e^{\alpha n} + c_s]^{1/n}$) or bitumen viscosity ($\mu_D = \mu/\mu_b = [(1 - c_s) + c_s e^{-\alpha n}]^{1/n}$), the R_{ac} value for a specific solvent/bitumen system is different. The integrals in eqs 13 and 14 do not have an analytical solution and should be evaluated numerically. Figure 2 shows the viscosity of bitumen/solvent mixtures for different solvents, and the obtained viscosity parameters for each system are presented in Table 2. It is evident from Figure 2 that the power-law mixing rule predicts the experimental data with acceptable accuracy.

The critical Rayleigh numbers for all of the mixtures using two different equations, obtained from the exponential viscosity mixing rule (EMR) and power-law mixing rule (PLMR), along with the one for the classical Horton–Rogers–Lapwood problem^{45,46} (for comparison), are presented in Figure 3. As shown, the critical Rayleigh number (defined based on μ_b) decreases with an increase in the natural log of mobility ratio, and the critical Rayleigh numbers are much smaller than the classical value of $4\pi^2$. In contrast, the R_{ac} increases with an increase in the natural log of mobility ratio for the case Rayleigh number defined based on μ_s . The results highlight the role of concentration dependency of viscosity on the mixing and dilution of bitumen by a solvent during bitumen leaching. As seen in Figure 3a,b, EMR leads to larger critical Rayleigh values compared to the PLMR. It has been previously demonstrated by Sabet et al.⁵² that the PLMR predicts the experimental mixture viscosity data at large viscosity ratios better than EMR while EMR overestimates the viscosity data. This difference (for a specific solvent/bitumen mixture) is due to the larger viscosity values predicted by EMR.

As shown by eq 1, the interfacial velocity varies linearly with the porous medium permeability. Likewise, the Sherwood number (Sh), which represents a measure of the convective to diffusive flux, scales linearly with the Ra number. This equation demonstrates that the gravity drainage rate is constant during the infinite-acting period (i.e., the time duration at which the top boundary has not been affected by the solvent yet) and independent of the formation height H .^{32,41,42}

As explained before, if the diffusion coefficient is assumed to be constant, eq 1 will be reduced to eq 5, where the interfacial

velocity is independent of the diffusion coefficient. Figure 4 shows the interfacial velocity of different bitumen/solvent mixtures against permeability in a log-log scale for this special case. As shown, the interfacial velocity increases with an increase in the permeability of the porous media. It should be noted that Mokrys³⁸ and Mokrys and Butler^{36,37} solvent chamber theory does not consider the asphaltene precipitation for *n*-alkane solvents.

The presented data are for different bitumen/solvent mixtures along with experimental data of Athabasca/toluene and Suncor/toluene conducted by Mokrys and Mokrys.³⁸ It is clear from Figure 4 that the constant diffusion assumption could predict the experimental data of Suncor/toluene with reasonable accuracy, while for the Athabasca/toluene, the interfacial velocity is underestimated. The interfacial velocity (eq 5) is directly proportional to the density difference of heavy and light fluids ($U \propto \Delta\rho$), and a higher density difference leads to a higher interfacial velocity. Moreover, the velocity is inversely proportional to the viscosity of the solution ($U \propto \Delta\mu$); hence, a lower solution viscosity results in a higher interfacial velocity.

Figure 5 shows the Sherwood number against the Rayleigh number for the constant molecular diffusion coefficient case. Sherwood number is defined as the ratio of mixing due to convection to mixing achieved by pure diffusion, and it is used as a dimensionless measure of dissolution efficiency.^{56,57} A Sherwood number close to unity represents the dominance of the diffusion mechanism. On the other hand, a Sherwood number of 10^3 implies that convective mixing is 10^3 times more efficient than diffusion. The large values of Sherwood numbers ($\sim 0.2 \times 10^1$ to 1×10^5) indicate that convection is the dominant process in the bitumen leaching by solvent. Therefore, it can be concluded from the results that convective dissolution plays a crucial role in enhancing the mass transfer between solvent and bitumen.

To calculate the Sherwood numbers from interface velocities for each mixture, the diffusion coefficients and height of the bitumen column are required. The molecular diffusion coefficients of solvent/bitumen are presented in Table 3. A linear mixing rule is used for multicomponent solvents ($D_{\text{smix}} = \sum x_{si} D_{si}$, where x_{si} is the mole fraction of component i). The height of the domain (H) was assumed to be 9 cm, equal to the height of the Hele-Shaw cell employed by Mokrys and Butler³⁸ in their experiments. As expected, Sh scales linearly with Ra for all mixtures with different β values depending on the physical properties of each solvent/bitumen system. The

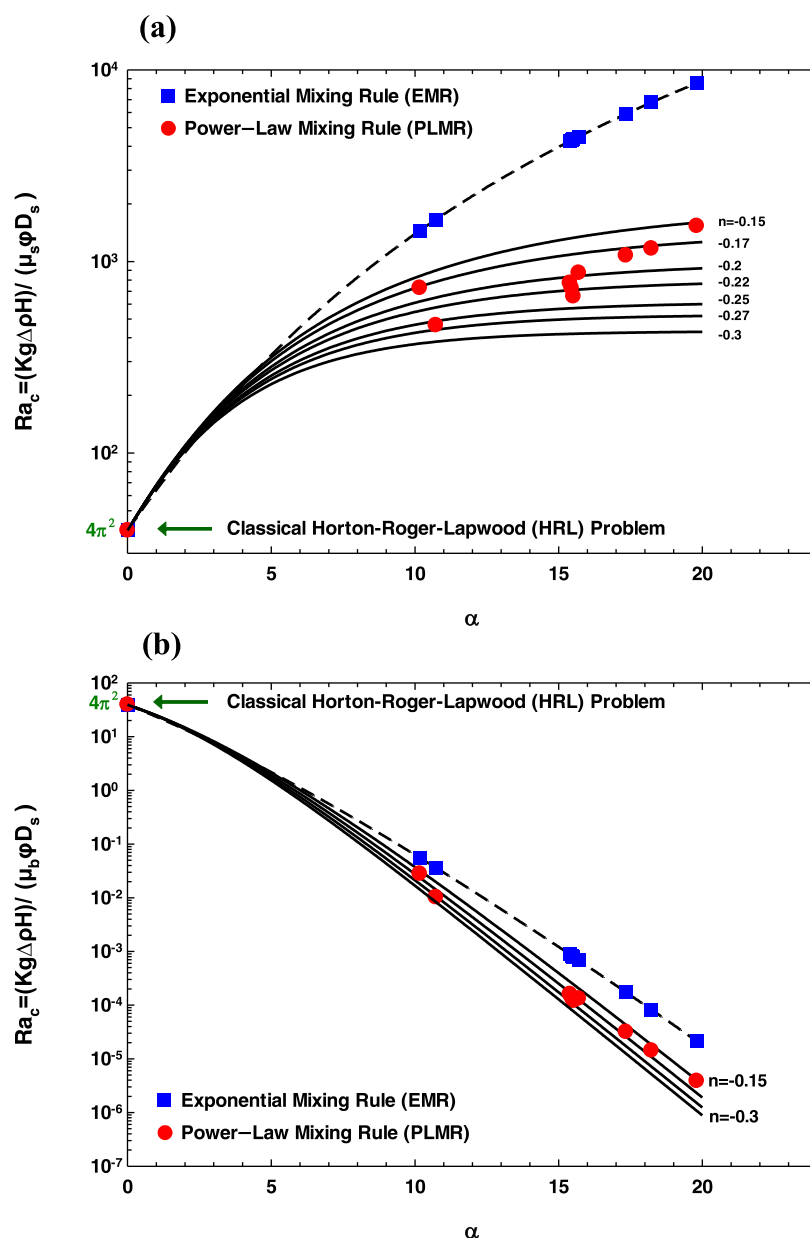


Figure 3. Critical Rayleigh number versus the natural log of mobility ratio for the onset of convective mixing for different systems. Rayleigh number is defined based on the viscosity of solvent (μ_s) in (a), while the viscosity of bitumen (μ_b) is used in (b). The blue squares represent the critical Rayleigh values of various solvent/bitumen systems, and the dashed line shows the general Ra_c for $\alpha = 0-20$ obtained using eqs 11 and 10, respectively. The red-filled circles show the Ra_c of different solvent/bitumen systems calculated by eq 12 in both graphs. The solid lines are plotted to represent the Ra_c trend using eq 12 for $\alpha = 0-20$ and different adjustable parameters range, n from -0.15 to -0.3 .

ethyl acetate case was excluded due to the absence of molecular diffusion data.

For the sake of completeness, the scaling behavior of Sh against Ra for simple counter-current flow, linear gradient model, exponential gradient model, and linear step function gradient model is demonstrated in Figure 6 (see Table 1 for a description of different models) to compare with the results obtained from the solvent chamber theory model. In the linear step function gradient model, it is assumed that solvent volume fraction (c_s) range across the boundary layer for Athabasca/toluene is $c_s = 0.33-0.38$;³⁸ for Suncor/toluene, this range is $c_s = 0.07-0.12$;³⁸ and for other mixtures, it is equal to an average of Athabasca/toluene and Suncor/toluene mixtures $c_s = 0.2-0.25$. As shown, similar to the solvent chamber theory model, the Sh scales linearly with Ra . However, the maximum value of

the Sherwood number for solvent chamber theory reaches $\sim 10^5$, whereas for the other models, the highest value is $\sim 6 \times 10^4$, which demonstrates a significant difference. Hence, it can be inferred that these models overestimate the experimental data. It is worthwhile to mention that the Ra number range is the same for all models and the difference between Sh values of the solvent chamber theory model and other models is due to the difference in their scaling prefactor (β) values, which will be discussed in detail later.

Figure 7a shows the behavior of the scaling prefactor (β) vs the natural log of mobility ratio (α) for the solvent chamber theory for all n values. The behavior of the scaling prefactor (β) for an average of all n values ($n_{\text{avg}} = -0.2019$) is also shown in Figure 7b. The experimental results of Mokrys are also shown for comparison. The results show that a lower

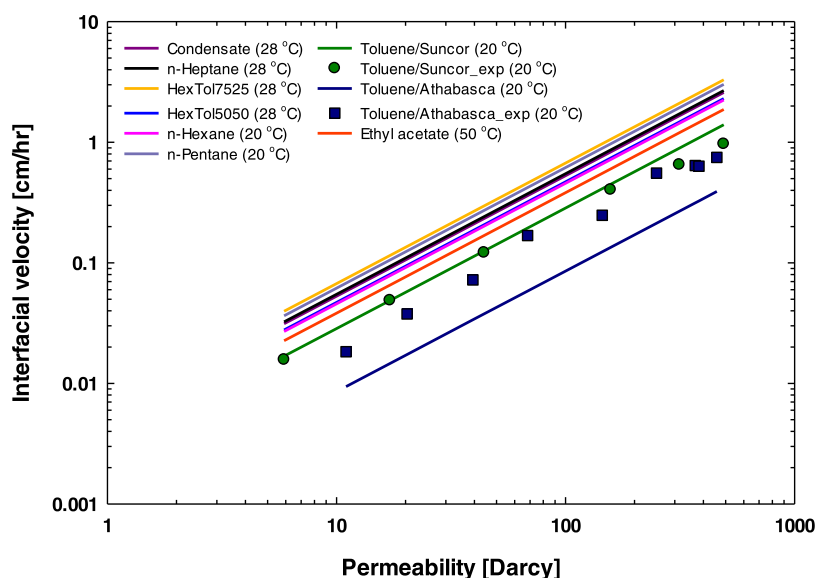


Figure 4. Interfacial velocity of different bitumen/solvent systems versus permeability of the porous medium. The experimental data of Athabasca/toluene (dark blue squares) and Suncor/toluene (green circles) at 20 °C are obtained from the previous experimental studies by Mokrys et al.³⁸

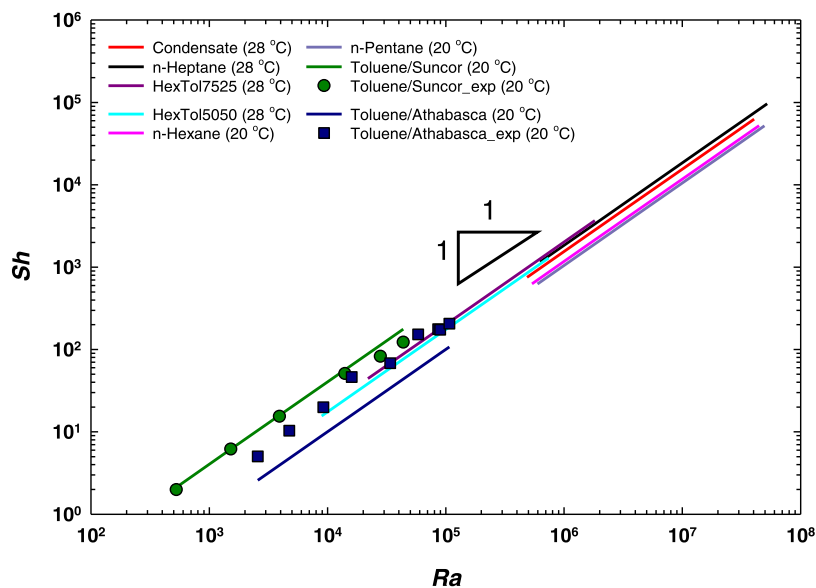


Figure 5. Sherwood number against the Rayleigh number (defined based on μ_s) for various solvent/bitumen mixtures was obtained using the solvent chamber theory. The Sherwood numbers of Athabasca/toluene (dark blue squares) and Suncor/toluene (green circles) at 20 °C are calculated using the experimental data provided by the previous experimental studies by Mokrys et al.³⁸

Table 3. Diffusion Coefficients of Solvent/Bitumen Mixtures

bitumen	solvent	diffusion coefficient [m^2/s]	ref
Athabasca	toluene	9.10×10^{-10}	Mokrys et al. ³⁸
MacKay	<i>n</i> -pentane	1.45×10^{-11}	Fu et al. ⁵⁸
Surmont	condensate	1.03×10^{-11}	mixing rule
MacKay	<i>n</i> -hexane	1.07×10^{-11}	Fu et al. ⁵⁸
Surmont	<i>n</i> -heptane	6.98×10^{-12}	Fu et al. ⁵⁸
MacKay	hextol 5050	4.45×10^{-10}	mixing rule
MacKay	hextol 7525	2.24×10^{-10}	mixing rule
Suncor	toluene	1.98×10^{-9}	Mokrys et al. ³⁸

mobility ratio α ($= \ln(\mu_b/\mu_s)$) results in a larger scaling prefactor (β), which corresponds to a higher rate of convective mass transfer ($Sh = \beta Ra$) at a specific Ra .

The scaling prefactor for all models against the natural log of mobility ratio is demonstrated in Figure 8. The results show that a higher natural log of mobility ratio corresponds to a lower scaling prefactor and eventually results in a lower convective mass transfer. It should be noted that all of the models show an exponential decay dependency of the scaling prefactor to the natural log of mobility ratio. The blue squares represent the acquired scaling prefactor of experimental data for Athabasca/toluene and Suncor/toluene. The results of various solvent/bitumen mixtures were obtained from the solvent chamber theory model. It can be inferred from the results that the solvent chamber theory model predicts the experimental data better than other models, and indeed, other models overestimate the experimental data.

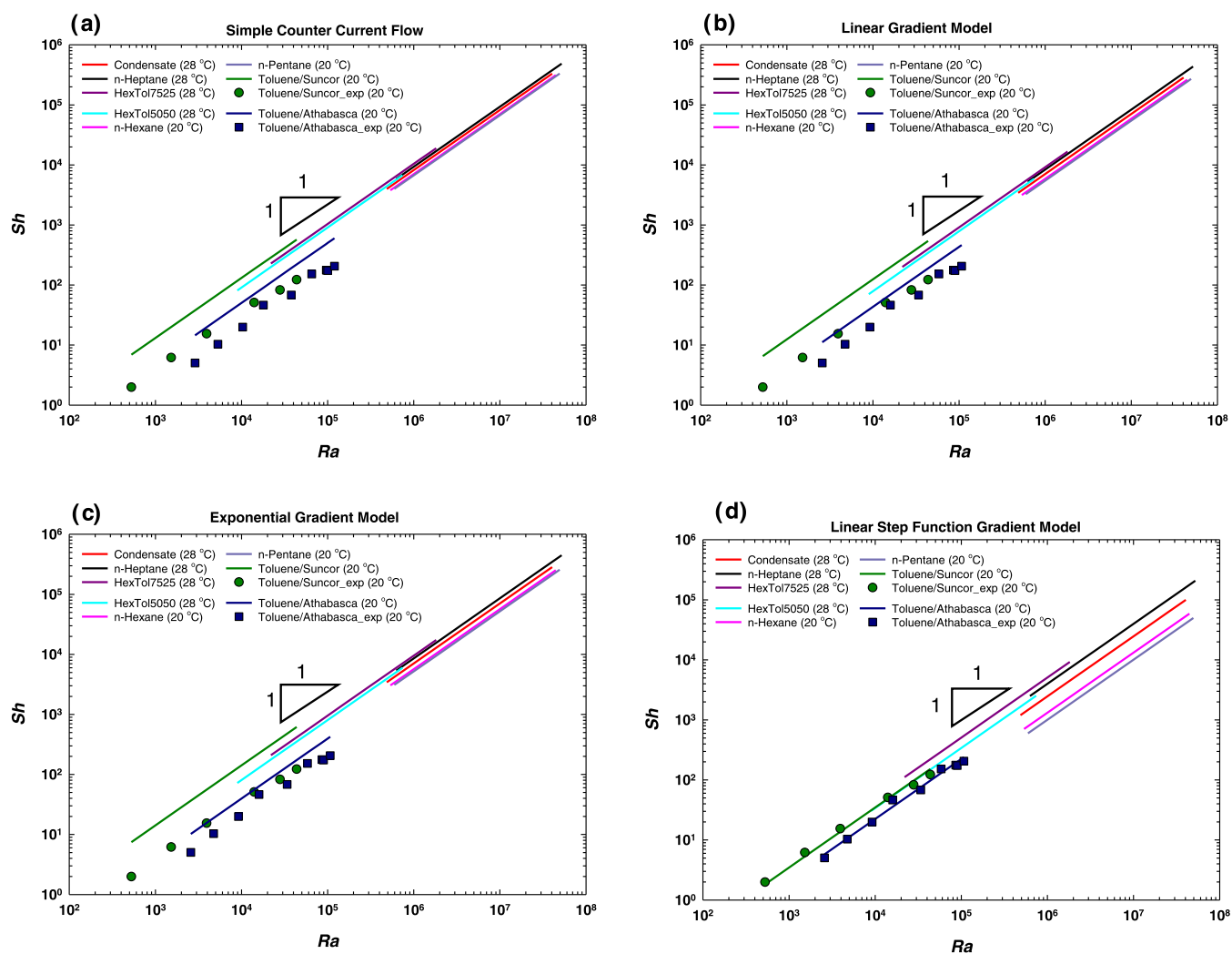


Figure 6. Sherwood number against the Rayleigh number (defined based on μ_s) using (a) simple counter-current flow, (b) linear gradient model, (c) exponential gradient model, and (d) linear step function gradient model for various solvent/bitumen mixtures.

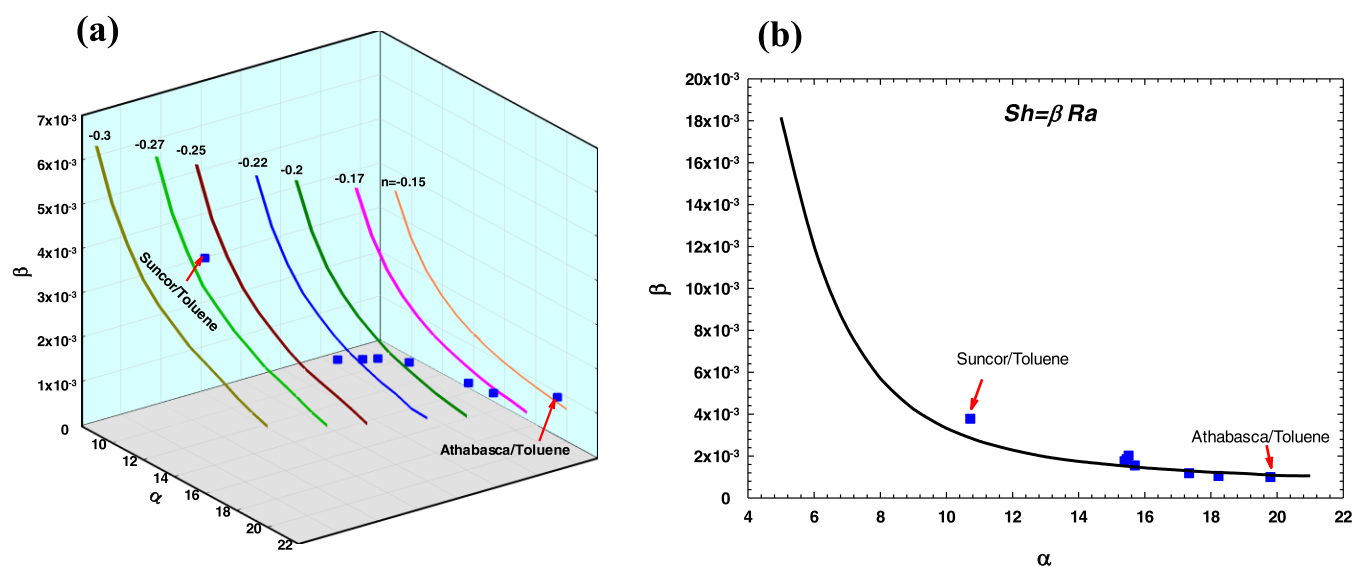


Figure 7. (a) Theoretical scaling prefactor (β) as a function of the natural log of mobility ratio (α) for the solvent chamber theory at different n values from -0.15 to -0.3 . (b) Theoretical scaling prefactor (β) as a function of the natural log of mobility ratio (α) for the solvent chamber theory at $n_{\text{avg}} = -0.2019$. The theory is compared with the results of various solvent/bitumen mixtures. The scaling prefactor (β) of Athabasca and Suncor (shown with red arrows) is calculated from the reported experimental data of Mokrys et al.³⁸

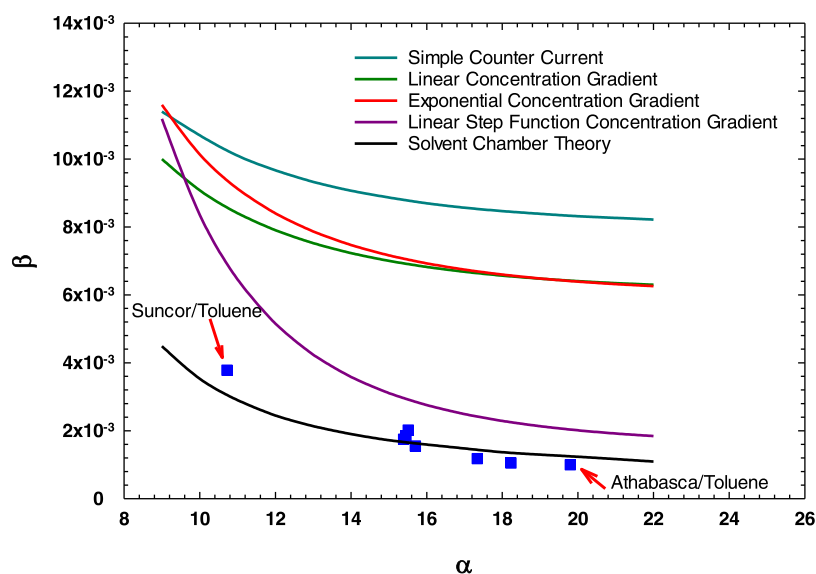


Figure 8. Theoretical scaling prefactor (β) as a function of the natural log of mobility ratio (α) for all models and compared with the obtained results of various solvent/bitumen mixtures using the solvent chamber theory (dark blue squares). The scaling prefactor (β) of Athabasca and Suncor (shown with red arrows) is obtained from experimental data of Mokrys et al.³⁸

4. SUMMARY AND CONCLUSIONS

In this study, we used Mokrys and Butler solvent chamber theory to study the bitumen production rate for various bitumen/solvent mixtures. The following conclusions can be drawn from this study:

- A linear scaling relation in the form of $Sh = \beta Ra$ that relates the Sherwood number (a measure of the convective dissolution of solvent in bitumen to pure diffusion flux) to the Rayleigh number for various solvents is presented.
- The large values of the obtained Sherwood numbers reveal that convective dissolution significantly increases the mass transfer between solvent and bitumen.
- It was determined that the Sherwood number is directly proportional to the density difference of bitumen and solvent and inversely to the viscosity of solution.
- It was shown that the scaling prefactor β decreases exponentially with the increase of mobility ratio ($\alpha = \ln(\mu_b/\mu_s)$); hence, a lower mobility ratio results in a larger value of β followed by a higher rate of convective mass transfer.
- The developed scaling relation reveals that bitumen drainage rate remains constant during the infinite-acting period (before the convection plumes reach the top boundary), highlighting the importance of solvent-aided bitumen leaching process for further field scale development considerations.
- The results of solvent chamber theory were compared with the simple counter-current flow model and the concentration gradient models. It was revealed that the solvent chamber theory could predict the experimental results better than other models.
- Our theoretical results of Sh vs Ra reveal that if enough drainage area is provided in the field scale application, for instance, through horizontal fractures, the solvent-aided leaching of bitumen is able to provide economical oil rates.
- The critical Rayleigh values were obtained based on two mixing rules, exponential mixing rule (EMR) and power-

law mixing rule (PLMR), and it was concluded that EMR-based equation gives a larger value of Ra_c due to the overestimation of mixture viscosity by EMR.

APPENDIX

A. Solvent Chamber Theory

The interfacial velocity is given by

$$U = Kg(\rho_b - \rho_s) \frac{[I_3 - (1 - c_{\max})I_2]}{I_1} \quad (\text{A.1})$$

in which

$$I_1 = \int_{c_{\min}}^{c_{\max}} \frac{D_s}{c_s} dc_s \quad (\text{A.2})$$

$$I_2 = \int_{c_{\min}}^{c_{\max}} \frac{D_s(1 - c_s)}{\mu c_s} dc_s \quad (\text{A.3})$$

$$I_3 = \int_{c_{\min}}^{c_{\max}} \frac{D_s(1 - c_s)^2}{\mu c_s} dc_s \quad (\text{A.4})$$

With a constant molecular diffusion coefficient, D_s will cancel out in these equations, and I_1 , I_2 , and I_3 are reduced to

$$I'_1 = \int_{c_{\min}}^{c_{\max}} \frac{1}{c_s} dc_s \quad (\text{A.5})$$

$$I'_2 = \int_{c_{\min}}^{c_{\max}} \frac{(1 - c_s)}{\mu c_s} dc_s \quad (\text{A.6})$$

$$I'_3 = \int_{c_{\min}}^{c_{\max}} \frac{(1 - c_s)^2}{\mu c_s} dc_s \quad (\text{A.7})$$

To make the equations dimensionless, we multiply both sides of eq A.1 by $H/D_s\mu_s$, so

$$\left[\frac{HU}{D_s\mu_s} \right] = \left[\frac{Kg\Delta\rho}{D_s\mu_s} \frac{[I'_3 - (1 - c_{\max})I'_2]}{I'_1} \right] \quad (\text{A.8})$$

Multiplying both sides by μ_s gives

$$\left[\frac{HU}{D_s} \right] = \left[\frac{Kg\Delta\rho H}{D_s\mu_s} \right] \left[\frac{\mu_s [I'_3 - (1 - c_{\max})I'_2]}{I'_1} \right] \quad (\text{A.9})$$

So, the left side results in the Sherwood number:

$$Sh = \frac{HU}{D_s} \quad (\text{A.10})$$

The first factor on the right side is the Rayleigh number,

$$Ra = \frac{K\Delta\rho gH}{D_s\mu_s} \quad (\text{A.11})$$

and the second factor is a constant, β , defined as

$$\beta = \left[\frac{I'_{D3} - (1 - c_{\max})I'_{D2}}{I'_1} \right] \quad (\text{A.12})$$

where I'_1 remains unchanged, and I'_{D2} and I'_{D3} are

$$I'_{D2} = \int_{c_{\min}}^{c_{\max}} \frac{(1 - c_s)}{\mu_D c_s} dc_s \quad (\text{A.13})$$

$$I'_{D3} = \int_{c_{\min}}^{c_{\max}} \frac{(1 - c_s)^2}{\mu_D c_s} dc_s \quad (\text{A.14})$$

where the dimensionless viscosity is $\mu_D = \mu/\mu_s$.

We define the viscosity as in eq A.15, where $\alpha = \ln M$, $M = \mu_b/\mu_s$, n is an adjustable parameter, and c_s is the solvent volume fraction. Thus, the dimensionless viscosity is

$$\mu_D = [(1 - c_s)e^{\alpha n} + c_s]^{1/n} \quad (\text{A.15})$$

and I'_1 , I'_{D2} , and I'_{D3} become

$$I'_1 = \int_{c_{\min}}^{c_{\max}} \frac{1}{c_s} dc_s = \ln \left(\frac{c_{\max}}{c_{\min}} \right) \quad (\text{A.16})$$

$$I'_{D2} = \int_{c_{\min}}^{c_{\max}} \frac{(1 - c_s)}{[(1 - c_s)e^{\alpha n} + c_s]^{1/n} c_s} dc_s \quad (\text{A.17})$$

$$I'_{D3} = \int_{c_{\min}}^{c_{\max}} \frac{(1 - c_s)^2}{[(1 - c_s)e^{\alpha n} + c_s]^{1/n} c_s} dc_s \quad (\text{A.18})$$

Therefore, eq A.12 for β reduces to

$$\beta = \frac{1}{\ln(c_{\max}/c_{\min})} \left[\int_{c_{\min}}^{c_{\max}} \frac{(1 - c_s)(c_{\max} - c_s)}{[(1 - c_s)e^{\alpha n} + c_s]^{1/n} c_s} dc_s \right] \quad (\text{A.19})$$

It should be noted that c_{\max} is a concentration that $\mu_D|_{c_s=c_{\max}} = 1 + c_{\max}$ and c_{\min} is a concentration that $f(c_s = c_{\min}) = c_s\mu_D/(1 - c_s)$ is maximum.

B. Simple Counter-Current Flow

In this model, the rate of rising of the bitumen interface only occurs by convection due to a simple counter-current flow. The effects of diffusion, shock fronts, and boundary layer are neglected. It provides an absolute upper limit to the rate at which upward leaching can occur. The details of the model can be found elsewhere.^{37,38}

The interfacial velocity is

$$U = KgF(X_c, c_s) \quad (\text{B.1})$$

$$F(X_c, c_s) = \frac{(1 - c_s)(\rho - \rho_s)(X_c - X_c^2)}{\mu X_c + \mu_s(1 - X_c)} \quad (\text{B.2})$$

where X_c is the fraction of the width containing solvent flow due to buoyancy. The function $F(X_c, c_s)$ is maximum at a specific solvent concentration. Since $F(X_c, c_s)$ is a function of two variables, the determination of this maximum value involves choosing a value of c_s and then finding $X_c = X_{\max}$ such that $F(X_c, c_s)$, and therefore U , are largest. The maximum of the $F(X_c, c_s)$, at a given solvent concentration, is at $X_c = X_{\max}$, where $(\partial F/\partial X_c)_{c_s}|_{X_c=X_{\max}} = 0$ then X_{\max} is

$$X_{\max} = \frac{1}{\sqrt{\frac{\mu}{\mu_s} + 1}} \quad (\text{B.3})$$

Using the density mixing rule, $\rho = \rho_b(1 + \gamma c_s)$ gives the dimensionless density as $\rho_D = \rho/\Delta\rho = -(1 + \gamma c_s)/\gamma$, where $\Delta\rho = \rho_b - \rho_s$ and $\gamma < 0$ is the coefficient of density, defining the dimensionless viscosity as $\mu_D = \mu/\mu_s$, and substituting $X_c = X_{\max}$ from eq B.3 into eq B.2, $F(X_{\max}, c_s)$ will be

$$F(X_{\max}, c_s) = \frac{\Delta\rho}{\mu_s} \left[\frac{1 - c_s}{\sqrt{\mu_D} + 1} \right]^2 \quad (\text{B.4})$$

And the interfacial velocity is

$$U = \frac{Kg\Delta\rho}{\mu_s} \left[\frac{1 - c_s}{\sqrt{\mu_D} + 1} \right]^2 \quad (\text{B.5})$$

To make the equations dimensionless, we multiply both sides of eq B.5 by H/D_s , so

$$\left[\frac{UH}{D_s} \right] = \left[\frac{Kg\Delta\rho H}{D_s\mu_s} \right] \left[\frac{1 - c_s}{\sqrt{\mu_D} + 1} \right]^2 \quad (\text{B.6})$$

So, the left side results in Sherwood number

$$Sh = \frac{UH}{D_s} \quad (\text{B.7})$$

The right side is Rayleigh number

$$Ra = \frac{K\Delta\rho gH}{D_s\mu_s} \quad (\text{B.8})$$

and the second term is a constant, β , as

$$\beta = \left[\frac{1 - c_s}{\sqrt{\mu_D} + 1} \right]^2 \quad (\text{B.9})$$

Therefore, eq B.5 in the dimensionless form is

$$Sh = \beta Ra \quad (\text{B.10})$$

C. Concentration Gradient Models

The concentration gradient model is divided into three different submodels, including linear, exponential, and linear step function. The mass transfer occurs across a boundary layer, and each model assumes a solvent concentration profile across the boundary layer to determine the interface rise velocity. Such a simplification enables the determination of individual contributions from density and viscosity to the total gravity flow within the boundary layer according to the chosen profile. The details of the model can be found elsewhere.^{37,38}

The interfacial velocity is obtained as

$$U = KgZ(X_{\max}) \quad (\text{C.1})$$

where $Z(X_{\max})$ is the maximum value of the function

$$Z(X_i) = \frac{A(1 - X_i)^2 + B(1 - X_i)X_i}{C(1 - X_i)X_i + D(1 - X_i)^2 + EX_i + F(1 - X_i)} \quad (\text{C.2})$$

where $A, B, C, D, E,$ and F are constants and are given as

$$A = N_d - \frac{N_a N_e}{N_b} \quad (\text{C.3})$$

$$B = \frac{\rho_s}{\mu_s} - \frac{N_a}{\mu_s N_b} \quad (\text{C.4})$$

$$C = \frac{N_c}{\mu_s N_b} - 1 \quad (\text{C.5})$$

$$D = \frac{N_c N_e}{N_b} - N_f \quad (\text{C.6})$$

$$E = -\frac{1}{\mu_s N_b} \quad (\text{C.7})$$

$$F = -\frac{N_e}{N_b} \quad (\text{C.8})$$

where the constants $N_a - N_e$ are called the solvent number integrals.

The value X_i at which the maximum value of function $Z(X_i)$ occurs is obtained by differentiating eq C.2 with respect to X_i . Doing this operation, $X_i = X_{\max}$ is then given by the expression

$$X_{\max} = -\frac{b}{2a} - \frac{\sqrt{b^2 - 4ac}}{2a} \quad (\text{C.9})$$

where

$$a = BF + AE - AF + BD - BE - AC \quad (\text{C.10})$$

$$b = 2(AF - BD - BF + AC) \quad (\text{C.11})$$

$$c = BD - AF + BF - AC - AE \quad (\text{C.12})$$

It is worthwhile mentioning that the constants $A-F$ and $a-c$ remain unchanged for all submodels, linear, exponential, and linear step function, but the solvent number integral constants ($N_a - N_e$) depend on the submodel.

To make the equations dimensionless, we multiply both sides of eq C.1 by $H\mu_s/D_s\mu_s$, and using the density mixing rule, $\rho = \rho_b(1 + \gamma c_s)$ gives the dimensionless density as $\rho_D = \rho/\Delta\rho = -(1 + \gamma c_s)/\gamma$, where $\Delta\rho = \rho_b - \rho_s$ and $\gamma < 0$ is the coefficient of density and the dimensionless viscosity as $\mu_D = \mu/\mu_s$, we will have

$$Sh = \beta Ra \quad (\text{C.13})$$

where Sh is the Sherwood number ($Sh = UH/D_s$), Ra is the Rayleigh number ($Ra = K\Delta\rho gH/D_s\mu_s$), and β is a constant defined as follows:

$$\beta = [A_D(1 - X_{\max})^2 + B_D(1 - X_{\max})X_{\max}] / [C_D(1 - X_{\max})X_{\max} + D_D(1 - X_{\max})^2 + E_D X_{\max} + F_D(1 - X_{\max})] \quad (\text{C.14})$$

where $A_D, B_D, C_D, D_D, E_D,$ and F_D are constants and are given as

$$A_D = N_{dD} - \frac{N_{aD}N_{eD}}{N_{bD}} \quad (\text{C.15})$$

$$B_D = -\frac{1 + \gamma}{\gamma} - \frac{N_{aD}}{N_{bD}} \quad (\text{C.16})$$

$$C_D = \frac{N_{cD}}{N_{bD}} - 1 \quad (\text{C.17})$$

$$D_D = \frac{N_{cD}N_{eD}}{N_{bD}} - N_{fD} \quad (\text{C.18})$$

$$E_D = -\frac{1}{N_{bD}} \quad (\text{C.19})$$

$$F_D = -\frac{N_{eD}}{N_{bD}} \quad (\text{C.20})$$

Equations C.9–C.12 are valid for the dimensionless form and can be used to determine X_{\max} and the dimensionless solvent number integral constants ($N_{aD} - N_{eD}$) depend on the submodel and will be defined in the following sections.

C.1. Linear Concentration Gradient. The principal assumption of this submodel is a linear concentration variation across the boundary layer for a steady-state flow.

$$c_s(\xi) = 1 - \frac{\xi}{\xi_{\max}} \quad (\text{C.1.1})$$

where ξ is the distance normal to the interface across the boundary layer. This equation expresses a linear concentration variation across the boundary layer for a steady-state flow and for $0 \leq \xi \leq \xi_{\max}$.

Thus, by applying this assumption, the solvent number integral constants in the dimensionless form are

$$N_{aD} = \int_{c_{\min}}^1 \frac{\rho_D(1 - c_s)}{\mu_D} dc_s \quad (\text{C.1.2})$$

$$N_{bD} = \int_{c_{\min}}^1 \frac{(1 - c_s)}{\mu_D} dc_s \quad (\text{C.1.3})$$

$$N_{cD} = \int_{c_{\min}}^1 (1 - c_s) dc_s \quad (\text{C.1.4})$$

$$N_{dD} = \int_{c_{\min}}^1 \frac{\rho_D c_s}{\mu_D} dc_s \quad (\text{C.1.5})$$

$$N_{eD} = \int_{c_{\min}}^1 \frac{c_s}{\mu_D} dc_s \quad (\text{C.1.6})$$

$$N_{fD} = \int_{c_{\min}}^1 c_s dc_s \quad (\text{C.1.7})$$

The minimum solvent concentration, c_{\min} , is set arbitrary at 0.05;³⁸ it is assumed that this is the minimum solvent concentration beyond which there is no significant drainage flow.

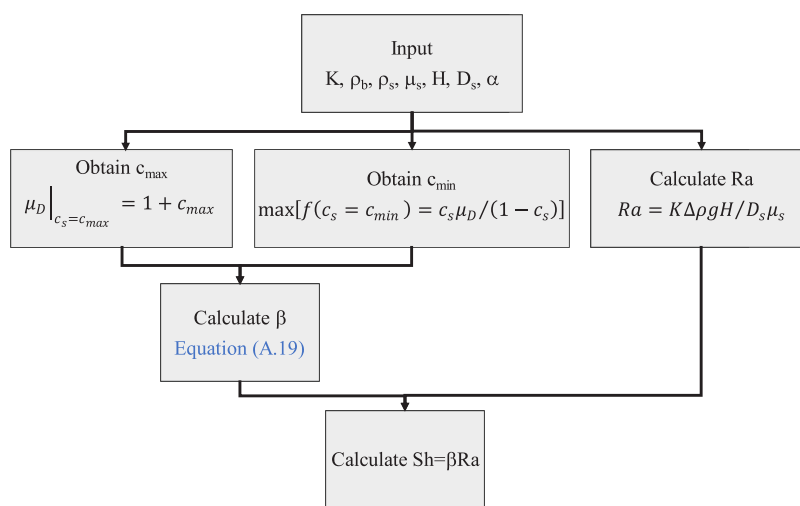
C.2. Exponential Concentration Gradient. If the steady-state solvent concentration c_s is assumed to change exponentially with the distance ξ across the boundary layer, and the assumption of $c_s = 0.05$ at $\xi = \xi_{\max}$ is valid, then

$$c_s(\xi) = e^{-2.996(\xi/\xi_{\max})} \quad (\text{C.2.1})$$

Table A1. Density of Raw Bitumen and Pure Solvents Used in the Density Equation $\rho = \rho_b(1 + \gamma c_s)$

bitumen	ρ_b [kg/m ³]	solvent	ρ_s [kg/m ³]	γ	temperature [°C]	ref
Athabasca	1028	toluene	866.9	-0.1567	20	Mokrys et al. ³⁸
MacKay	1008	<i>n</i> -pentane	625.75	-0.3792	20	Haddadnia et al. ⁵³
Surmont	1007	condensate ^a	672.75	-0.3325	26	Nourozieh et al. ⁵⁵
MacKay	1008	<i>n</i> -hexane	659.36	-0.3459	20	Haddadnia et al. ⁵³
Surmont	1007	<i>n</i> -heptane	678.95	-0.3258	28	Nourozieh et al. ⁵⁴
MacKay	1007	hextol 5050 ^b	747.8	-0.2574	28	this work
MacKay	1007	hextol 7525 ^c	696.1	-0.3087	28	this work
Suncor	1000	toluene	866.9	-0.1331	20	Mokrys et al. ³⁸
MacKay	986	ethyl acetate	863.18	-0.1246	50	Zirahi et al. ¹⁹

^aCondensate: *n*-C₅ (35.73 wt %), *n*-C₆ (25.29 wt %), *n*-C₇ (21.92 wt %), and C₈⁺ (17.06 wt %). ^bHextol 5050: *n*-C₆ (50 wt %) and toluene (50 wt %). ^cHextol 7525: *n*-C₆ (75 wt %) and toluene (25 wt %).

Figure A1. Algorithm used for the *Sh* calculations using solvent chamber theory.

Therefore, the solvent number integral constants in the dimensionless form will be

$$N_{aD} = \frac{1}{2.996} \int_{c_{\min}}^1 \frac{\rho_D(1 - c_s)}{\mu_D c_s} dc_s \quad (\text{C.2.2})$$

$$N_{bD} = \frac{1}{2.996} \int_{c_{\min}}^1 \frac{(1 - c_s)}{\mu_D c_s} dc_s \quad (\text{C.2.3})$$

$$N_{cD} = \frac{1}{2.996} \int_{c_{\min}}^1 \frac{(1 - c_s)}{c_s} dc_s \quad (\text{C.2.4})$$

$$N_{dD} = \frac{1}{2.996} \int_{c_{\min}}^1 \frac{\rho_D}{\mu_D} dc_s \quad (\text{C.2.5})$$

$$N_{eD} = \frac{1}{2.996} \int_{c_{\min}}^1 \frac{1}{\mu_D} dc_s \quad (\text{C.2.6})$$

$$N_{fD} = \frac{1}{2.996} \int_{c_{\min}}^1 dc_s \quad (\text{C.2.7})$$

C.3. Linear Step Function Concentration Gradient Model. If the solvent concentration gradient is assumed to vary linearly across the boundary layer (i.e., from c_{\max} ($\zeta = 0$) to c_{\min} ($\zeta = \zeta_{\max}$)), then c_s is

$$c_s = c_{\max} - \frac{c_{\max} - c_{\min}}{\zeta_{\max}} \zeta \quad (\text{C.3.1})$$

This equation approximates a step function for the solvent concentration across the boundary layer.

Thus, by applying this assumption, the solvent number integral constants in the dimensionless form are

$$N_{aD} = \frac{1}{c_{\max} - c_{\min}} \int_{c_{\min}}^{c_{\max}} \frac{\rho_D(1 - c_s)}{\mu_D} dc_s \quad (\text{C.3.2})$$

$$N_{bD} = \frac{1}{c_{\max} - c_{\min}} \int_{c_{\min}}^{c_{\max}} \frac{(1 - c_s)}{\mu_D} dc_s \quad (\text{C.3.3})$$

$$N_{cD} = \frac{1}{c_{\max} - c_{\min}} \int_{c_{\min}}^{c_{\max}} (1 - c_s) dc_s \quad (\text{C.3.4})$$

$$N_{dD} = \frac{1}{c_{\max} - c_{\min}} \int_{c_{\min}}^{c_{\max}} c_s \frac{\rho_D}{\mu_D} dc_s \quad (\text{C.3.5})$$

$$N_{eD} = \frac{1}{c_{\max} - c_{\min}} \int_{c_{\min}}^{c_{\max}} \frac{c_s}{\mu_D} dc_s \quad (\text{C.3.6})$$

$$N_{fD} = \frac{1}{c_{\max} - c_{\min}} \int_{c_{\min}}^{c_{\max}} c_s dc_s \quad (\text{C.3.7})$$

D. Density

The densities of various kinds of raw bitumen and data for the solvents used in the density equation $\rho = \rho_b(1 + \gamma c_s)$ are provided in Table A1.

E. Sherwood Number Calculation Algorithm

The algorithm used in the Sherwood number calculations using Solvent Chamber Theory is presented in Figure A1.

AUTHOR INFORMATION

Corresponding Author

Hassan Hassanzadeh – Department of Chemical and Petroleum Engineering, Schulich School of Engineering, University of Calgary, Calgary, Alberta T2N 1N4, Canada; orcid.org/0000-0002-3029-6530; Phone: +1 403 210 6645; Email: hhassanz@ucalgary.ca; Fax: +1 403 284 4852

Authors

Mohammadjavad Mohammadi – Department of Chemical and Petroleum Engineering, Schulich School of Engineering, University of Calgary, Calgary, Alberta T2N 1N4, Canada; orcid.org/0000-0001-6394-2167

Nasser Sabet – Department of Chemical and Petroleum Engineering, Schulich School of Engineering, University of Calgary, Calgary, Alberta T2N 1N4, Canada

Complete contact information is available at:

<https://pubs.acs.org/10.1021/acsomega.2c07634>

Notes

The authors declare no competing financial interest.

ACKNOWLEDGMENTS

The authors acknowledge the financial support from the Natural Sciences and Engineering Research Council of Canada (NSERC) and all of the member companies of the SHARP Research Consortium: Canadian Natural Resources Ltd., Cenovus Energy, CNOOC International, Husky Energy, Imperial Oil Limited, Kuwait Oil Company, Osum Oil Sands, Strathcona Resources Ltd., and Suncor Energy. The support of the Department of Chemical and Petroleum Engineering and the Schulich School of Engineering at the University of Calgary is also acknowledged.

NOMENCLATURE

Roman Symbols

α	natural log of mobility ratio [dimensionless]
β	scaling prefactor [dimensionless]
γ	coefficient in density relation [dimensionless]
ξ	normal distance in the boundary layer [L]
ξ_{\max}	width of boundary layer [L]
μ	viscosity [M/LT]
ρ	density [M/L ³]
$\Delta\rho$	density difference [M/L ³]
ϕ	porosity [dimensionless]

LETTERS

A	constant [T/L ²]
a	constant [dimensionless]
B	constant [T/L ²]
b	constant [dimensionless]
C	constant [dimensionless]
c	volume fraction [dimensionless] and constant [dimensionless]
Δc	concentration difference [M/L ³]
D	constant [dimensionless]
D_s	diffusion coefficient [L ² /T]

E	constant [dimensionless]
F	constant [dimensionless]
F_c	mass flux [M/L ² T]
F_{II}	integral function [dimensionless]
g	gravitational acceleration [L/T ²]
H	height of the Hele-Shaw cell [L]
I_1	integral constant [L ² /T]
I_2	integral constant [L ³ /M]
I_3	integral constant [L ³ /M]
K	permeability [L ²]
M	mobility ratio [dimensionless]
n	power-law mixing rule adjustable parameter [dimensionless]
N_a	solvent number integral [T/L ²]
N_b	solvent number integral [TL/M]
N_c	solvent number integral [dimensionless]
N_d	solvent number integral [T/L ²]
N_e	solvent number integral [dimensionless]
N_f	solvent number integral [dimensionless]
Ra	Rayleigh number [dimensionless]
Sh	Sherwood number [dimensionless]
U	interface velocity [L/T]
ν	natural buoyancy flux [L/T]
X_c	fraction of the width containing solvent [dimensionless]
X	mole fraction [dimensionless]
X_{II}	integral Function [dimensionless]
Y_{II}	constant [dimensionless]
z	vertical coordinate direction [L]

ACRONYMS

CSS	cyclic steam stimulation
DME	dimethyl ether
EA	ethyl acetate
EMR	exponential mixing rule
ES-SAGD	expanding-solvent steam-assisted gravity drainage
GHG	greenhouse gases
LSA	linear stability analysis
PLMR	power-law mixing rule
RT	Rayleigh–Taylor
SAGD	steam-assisted gravity drainage
SF	steam flooding
SOR	steam–oil ratio

SUBSCRIPTS

b	bitumen
c	critical
D	dimensionless
max	maximum (lower shock front)
min	minimum (upper shock front)
S	solvent

SUPERSCRIPTS

'	constant diffusion property
---	-----------------------------

REFERENCES

- (1) Speight, J. *Enhanced Recovery Methods for Heavy Oil and Tar Sands*, 2nd ed.; Elsevier, 2016.
- (2) Dong, X.; Liu, H.; Chen, Z.; Wu, K.; Lu, N.; Zhang, Q. Enhanced Oil Recovery Techniques for Heavy Oil and Oilsands Reservoirs after Steam Injection. *Appl. Energy* **2019**, *239*, 1190–1211.
- (3) Bao, Y.; Wang, J.; Gates, I. D. On the Physics of Cyclic Steam Stimulation. *Energy* **2016**, *115*, 969–985.

- (4) Rabiei Faradonbeh, M.; Hassanzadeh, H.; Harding, T. Numerical Simulations of Bitumen Recovery Using Solvent and Water Assisted Electrical Heating. *Fuel* **2016**, *186*, 68–81.
- (5) Hassanzadeh, H.; Harding, T. Analysis of Conductive Heat Transfer during In-Situ Electrical Heating of Oil Sands. *Fuel* **2016**, *178*, 290–299.
- (6) Nasr, T.; Beaulieu, G.; Golbeck, H.; Heck, G. Novel Expanding Solvent-SAGD Process “ES-SAGD”. *J. Can. Pet. Technol.* **2003**, *42*, 13–16.
- (7) Ahmadi, M. A.; Zendeboudi, S.; Bahadori, A.; James, L.; Lohi, A.; Elkamel, A.; Chatzis, I. Recovery Rate of Vapor Extraction in Heavy Oil Reservoirs - Experimental, Statistical, and Modeling Studies. *Ind. Eng. Chem. Res.* **2014**, *53*, 16091–16106.
- (8) Sherratt, J.; Sharifi Haddad, A.; Rafati, R. Hot Solvent-Assisted Gravity Drainage in Naturally Fractured Heavy Oil Reservoirs: A New Model and Approach to Determine Optimal Solvent Injection Temperature. *Ind. Eng. Chem. Res.* **2018**, *57*, 3043–3058.
- (9) Kahrobaei, S.; Farajzadeh, R.; Suicmez, V. S.; Bruining, J. Gravity-Enhanced Transfer between Fracture and Matrix in Solvent-Based Enhanced Oil Recovery. *Ind. Eng. Chem. Res.* **2012**, *51*, 14555–14565.
- (10) Shokrollahi, A.; Majidi, S. M. J.; Ghazanfari, M. H. Monitoring and Characterizing the Finger Patterns Developed by Miscible Displacement in Fractured Heavy Oil Systems. *Ind. Eng. Chem. Res.* **2013**, *52*, 10853–10863.
- (11) Das, S. K.; Butler, R. M. Mechanism of the Vapor Extraction Process for Heavy Oil and Bitumen. *J. Pet. Sci. Eng.* **1998**, *21*, 43–59.
- (12) Haddadnia, A.; Zirrahi, M.; Hassanzadeh, H.; Abedi, J. In *Dimethylether-A Promising Solvent for ES-SAGD*, SPE Canada Heavy Oil Technical Conference, 2018; p 10.
- (13) Al-Murayri, M. T.; Maini, B. B.; Harding, T. G.; Oskouei, J. Multicomponent Solvent Co-Injection with Steam in Heavy and Extra-Heavy Oil Reservoirs. *Energy Fuels* **2016**, *30*, 2604–2616.
- (14) Gupta, S.; Gittins, S.; Picherack, P. Field Implementation of Solvent Aided Process. *J. Can. Pet. Technol.* **2005**, *44*, 8–13.
- (15) Gupta, S.; Gittins, S.; Christina Lake Solvent Aided Process Pilot. *J. Can. Pet. Technol.* **2006**, *45*, 15–18.
- (16) Abdi, M.; Zirrahi, M.; Hassanzadeh, H. Vapor-Liquid-Liquid Equilibrium Modeling of Water/Bitumen/Solvent (C1, C2, C3, and n-C4) Mixtures Using a Cubic-Plus-Association Equation of State. *Ind. Eng. Chem. Res.* **2022**, *61*, 8279–8292.
- (17) Shu, W. R.; Hartman, K. Effect of Solvent on Steam Recovery of Heavy Oil. *SPE Reservoir Eng.* **1988**, *3*, 457–465.
- (18) Deng, X. In *Recovery Performance and Economics of Steam/Propane Hybrid Process*, SPE International Thermal Operations and Heavy Oil Symposium, 2005; p 7.
- (19) Zirrahi, A.; Yamchi, H. S.; Haddadnia, A.; Zirrahi, M.; Hassanzadeh, H.; Abedi, J. Ethyl Acetate as a Bio-Based Solvent to Reduce Energy Intensity and CO₂ Emissions of In-Situ Bitumen Recovery. *AIChE J.* **2019**, *66*, No. e16828.
- (20) Zirrahi, A.; Yamchi, H. S.; Haddadnia, A.; Zirrahi, M.; Hassanzadeh, H.; Abedi, J. 2-D Physical Model Experimental Study of Ethyl Acetate and Steam Co-Injection for in-Situ Bitumen Recovery. *Fuel* **2020**, *265*, No. 116943.
- (21) Haddadnia, A.; Azinfar, B.; Zirrahi, M.; Hassanzadeh, H.; Abedi, J. Thermophysical Properties of Dimethyl Ether/Athabasca Bitumen System. *Can. J. Chem. Eng.* **2018**, *96*, 597–604.
- (22) Sheng, K.; Okuno, R.; Wang, M. In *Water-Soluble Solvent as an Additive to Steam for Improved SAGD*, SPE Canada Heavy Oil Technical Conference; OnePetro, 2017; pp 215–239.
- (23) Sheng, K.; Okuno, R.; Wang, M. Dimethyl Ether as an Additive to Steam for Improved Steam-Assisted Gravity Drainage. *SPE J.* **2018**, *23*, 1201–1222.
- (24) Yamchi, H. S.; Zirrahi, M.; Hassanzadeh, H.; Abedi, J.; Fadaei, H. Effect of Additives on Liquid–Liquid Equilibrium Properties of Butane/Bitumen Systems with Applications to Solvent Aided Bitumen Recovery Processes. *Chem. Eng. Res. Des.* **2018**, *137*, 452–460.
- (25) Govind, P. A.; Das, S.; Srinivasan, S.; Wheeler, T. J. In *Expanding Solvent SAGD in Heavy Oil Reservoirs*, International Thermal Operations and Heavy Oil Symposium; Heavy Oil: Integrating the Pieces, 2008; Vol. 1, pp 541–554.
- (26) Zare, A.; Abdulhameed, F. M.; Hesland, B.; Hamouda, A. A. Enhanced Heavy Oil Recovery (SAGD), Coinjection of Steam and Solvent, Reduction of CEOR and CSOR. *Pet. Sci. Technol.* **2017**, *35*, 570–577.
- (27) Ardali, M.; Mamora, D. D.; Barrufet, M. In *A Comparative Simulation Study of Addition of Solvents to Steam in SAGD Process*, Canadian Unconventional Resources and International Petroleum Conference, 2010; pp 2956–2971.
- (28) Nasr, T.; Ayodele, O. In *New Hybrid Steam-Solvent Processes for the Recovery of Heavy Oil and Bitumen*, Abu Dhabi International Petroleum Exhibition and Conference, 2006.
- (29) Sabet, N.; Hassanzadeh, H.; Abedi, J. Selection of Efficient Solvent in Solvent-Aided Thermal Recovery of Bitumen. *Chem. Eng. Sci.* **2017**, *161*, 198–205.
- (30) Khaledi, R.; Boone, T. J.; Motahhari, H. R.; Subramanian, G. In *Optimized Solvent for Solvent Assisted-Steam Assisted Gravity Drainage (SA-SAGD) Recovery Process*, SPE Canada Heavy Oil Technical Conference; OnePetro, 2015; pp 1000–1023.
- (31) Khaledi, R.; Motahhari, H. R.; Boone, T. J.; Fang, C.; Coutee, A. S. In *Azeotropic Heated Vapour Extraction- A New Thermal-Solvent Assisted Gravity Drainage Recovery Process*, SPE Canada Heavy Oil Technical Conference; OnePetro, 2018; p 20.
- (32) Santa, M. L. S.; Sabet, N.; Hassanzadeh, H. Propane-Aided Leaching of Bitumen from Oilsands. *Energy Fuels* **2020**, *34*, 5798–5803.
- (33) Rayleigh, L. Investigation of the Character of the Equilibrium of an Incompressible Heavy Fluid of Variable Density. *Proc. London Math. Soc.* **1882**, *s1-14*, 170–177.
- (34) Taylor, G. The Instability of Liquid Surfaces When Accelerated in a Direction Perpendicular to Their Planes. I. *Proc. R. Soc. London, Ser. A* **1950**, *201*, 192–196.
- (35) Saffman, P. G.; Taylor, G. The Penetration of a Fluid into a Porous Medium or Hele-Shaw Cell Containing a More Viscous Liquid. *Proc. R. Soc. London, Ser. A* **1958**, *245*, 312–329.
- (36) Mokrys, I. J.; Butler, R. M. The Rise of Interfering Solvent Chambers: Solvent Analog Model Of Steam-Assisted Gravity Drainage. *J. Can. Pet. Technol.* **1993**, *32*, 26–36, DOI: 10.2118/93-03-02.
- (37) Butler, R. M.; Mokrys, I. J. Solvent Analog Model of Steam-Assisted Gravity Drainage. *AOSTRA J. Res.* **1989**, *05*, No. 17.
- (38) Mokrys, I. J. *The Rise of Interfering Solvent Chambers: Solvent Analog Model of SAGD*, MSc. Thesis. University of Calgary, 1989.
- (39) Sabet, N.; Hassanzadeh, H.; De Wit, A.; Abedi, J. Scalings of Rayleigh-Taylor Instability at Large Viscosity Contrasts in Porous Media. *Phys. Rev. Lett.* **2021**, *126*, No. 094501.
- (40) Nenniger, J. E.; Dunn, S. G. In *How Fast Is Solvent Based Gravity Drainage?*, Canadian International Petroleum Conference; Petroleum Society of Canada, 2008.
- (41) Neufeld, J. A.; Hesse, M. A.; Riaz, A.; Hallworth, M. A.; Tchelepi, H. A.; Huppert, H. E. Convective Dissolution of Carbon Dioxide in Saline Aquifers. *Geophys. Res. Lett.* **2010**, *37* (22), L22404.
- (42) Howard, L. N. Convection at High Rayleigh Number. In *Applied Mechanics*; Springer, 1966; pp 1109–1115.
- (43) Meybodi, H. E.; Hassanzadeh, H. Mixing Induced by Buoyancy-Driven Flows in Porous Media. *AIChE J.* **2013**, *59*, 1378–1389.
- (44) Hassanzadeh, H.; Pooladi-Darvish, M.; Keith, D. W. The Effect of Natural Flow of Aquifers and Associated Dispersion on the Onset of Buoyancy-Driven Convection in a Saturated Porous Medium. *AIChE J.* **2009**, *55*, 475–485.
- (45) Horton, C. W.; Rogers, F. T. Convection Currents in a Porous Medium. *J. Appl. Phys.* **1945**, *16*, 367–370.
- (46) Lapwood, E. R. Convection of a Fluid in a Porous Medium. *Math. Proc. Cambridge Philos. Soc.* **1948**, *44*, 508–521.

- (47) Sabet, N.; Hassanzadeh, H.; Abedi, J. A New Insight into the Stability of Variable Viscosity Diffusive Boundary Layers in Porous Media under Gravity Field. *AIChE J.* **2018**, *64*, 1083–1094.
- (48) Faradonbeh, M. R.; Harding, T. G.; Abedi, J.; Hassanzadeh, H. Stability Analysis of Coupled Heat and Mass Transfer Boundary Layers During Steam–Solvent Oil Recovery Process. *Transp. Porous Media* **2015**, *108*, 595–615.
- (49) Butler, R. M.; Mokrys, I. J.; Herra, P. S. Natural Convection Effects in the Contacting of Bitumen with Diluents. *AOSTRA J. Res.* **1986**, *2*, 147–153.
- (50) Sabet, N.; Hassanzadeh, H.; Abedi, J. Stability of Gravitationally Unstable Double Diffusive Transient Boundary Layers with Variable Viscosity in Porous Media. *AIChE J.* **2017**, *63*, 2471–2482.
- (51) Koval, E. J. A Method for Predicting the Performance of Unstable Miscible Displacement in Heterogeneous Media. *Soc. Pet. Eng. J.* **1963**, *3*, 145–154.
- (52) Sabet, N.; Mohammadi, M.; Zirahi, A.; Zirrahi, M.; Hassanzadeh, H.; Abedi, J. Numerical Modeling of Viscous Fingering during Miscible Displacement of Oil by a Paraffinic Solvent in the Presence of Asphaltene Precipitation and Deposition. *Int. J. Heat Mass Transfer* **2020**, *154*, No. 119688.
- (53) Haddadnia, A.; Zirrahi, M.; Hassanzadeh, H.; Abedi, J. Thermo-Physical Properties of n-Pentane/Bitumen and n-Hexane/Bitumen Mixture Systems. *Can. J. Chem. Eng.* **2018**, *96*, 339–351.
- (54) Nourozieh, H.; Kariznovi, M.; Abedi, J. Modeling and Measurement of Thermo-Physical Properties for Athabasca Bitumen and n-Heptane Mixtures. *Fuel* **2015**, *157*, 73–81.
- (55) Nourozieh, H.; Kariznovi, M.; Abedi, J. Viscosity Measurement and Modeling for Mixtures of Athabasca Bitumen/n-Pentane at Temperatures up to 200 °C. *SPE J.* **2015**, *20*, 226–238.
- (56) Hassanzadeh, H.; Pooladi-Darvish, M.; Keith, D. W. Scaling Behavior of Convective Mixing, with Application to Geological Storage of CO₂. *AIChE J.* **2007**, *53*, 1121–1131.
- (57) De Paoli, M.; Zonta, F.; Soldati, A. Rayleigh-Taylor Convective Dissolution in Confined Porous Media. *Phys. Rev. Fluids* **2019**, *4*, No. 023502.
- (58) Fu, B. C. H.; Phillips, C. R. New Technique for Determination of Diffusivities of Volatile Hydrocarbons in Semi-Solid Bitumen. *Fuel* **1979**, *58*, 557–560.